Article

Predictive Modeling the Free Hydraulic Jumps Pressure through Advanced Statistical Methods

Seyed Nasrollah Mousavi [1], Renato Steinke Júnior [2], Eder Daniel Teixeira [2] and Daniele Bocchiola [3], Narjes Nabipour [4*], Amir Mosavi [5,6], Shahabodin Shamshirband [7,8*]

[1] Department of hydraulic Engineering, University of Tabriz, Tabriz 5166616471, Iran; s.n.mousavi@tabrizu.ac.ir
[2] Departamento de Obras Hidráulicas (DOH), Universidade Federal do Rio Grande do Sul, Porto Alegre, RS 90.040-000, Brazil; renato.steinkejunior@gmail.com; eder.teixeira@ufrgs.br
[3] Department of Civil and Environmental Engineering (DICA), Politecnico di Milano, L. da Vinci, 32, 20133, Milano, Italy; daniele.bocchiola@polimi.it
[4] Institute of Research and Development, Duy Tan University, Da Nang 550000, Vietnam
[5] Queensland University of Technology, 130 Victoria Park Road, Queensland 4059, Australia
[6] Kalman Kando Faculty of Electrical Engineering, Obuda University, 1034 Budapest, Hungary
[7] Department for Management of Science and Technology Development, Ton Duc Thang University, Ho Chi Minh City, Viet Nam shahaboddin.shamshirband@tdtu.edu.vn
[8] Faculty of Information Technology, Ton Duc Thang University, Ho Chi Minh City, Viet Nam
* Correspondence: shahaboddin.shamshirband@tdtu.edu.vn

Abstract: Pressure fluctuations beneath hydraulic jumps downstream of Ogee spillways potentially damage stilling basin beds. This paper deals with the extreme pressures underneath free hydraulic jumps along a smooth stilling basin. The experiments were conducted in a laboratory flume. From the probability distribution of measured instantaneous pressures, the pressures with different non-exceedance probabilities ($P^*_{a\%}$) could be determined. It was verified that the maximum pressure fluctuations, as well as the negative pressures, are located at the positions closest to the spillway toe. The minimum pressure fluctuations are located at the downstream of hydraulic jumps. It was possible to assess the cumulative curves of $P^*_{a\%}$ related to the characteristic points along the basin, and different Froude numbers. To benchmark the results, the dimensionless forms of mean pressures, standard deviations, and pressures with different non-exceedance probabilities were assessed. It was found that an existing methodology can be used to interpret the present data, and pressure distribution in similar conditions, by using a new third-order polynomial relationship for the standard deviation (σ^*x) with the determination coefficient (R^2) equal to 0.717. It was verified that the new optimized adjustment gives more accurate results for the estimation of the maximum extreme pressures than the minimum extreme pressures.

Keywords: mathematical modeling; characteristic points; extreme pressure; hydraulic jump; pressure fluctuations; standard deviation; stilling basin

1. Introduction

Knowledge of pressure fluctuations and extreme pressures allows for a better understanding of the energy dissipation process along the hydraulic jump. Pressure fluctuation underneath hydraulic jumps has been the subject of many studies. Notable early studies on pressure fluctuations are such as those by Bukreyev [1]; Locher [2]; Schiebe [3]; Abdul Khader and Elango [4]; Lopardo et al. [5]; Toso and Bowers [6]; Farhoudi and Narayanan [7]; Fiorotto and Rinaldo [8]; Fiorotto and Rinaldo [9]; Armenio et al. [10].

According to Yan et al. [11], the pressure fluctuations coefficient (C'_P) and peak frequencies of the spatial hydraulic jumps are higher than the classical jumps. Onitsuka et al. [12] found that roller oscillations affect the instantaneous flow depth and bed pressure. In addition, the instantaneous bed pressures are associated with free surface fluctuations. Lian et al. [13] stated that the fluctuating pressure spectrum in the rolling area follows the gravity similarity law. Lopardo and Romagnoli [14] used C'_P coefficient values to estimate the turbulence intensities in the region close to the stilling basin bed. Lopardo [15] proposed a relationship between the turbulence intensity and C'_P coefficient to determine the extreme maximum positive velocities close to the stilling basin bed for the low incident Froude numbers. Wang et al. [16] predicted the total pressure based upon the void fraction and velocity data, and the results were in good agreement with the experimental data. Firotto et al. [17] studied the stability of a plunge pool bottom under the fully developed jets and offered a design method to define the concrete thickness of plunge pool linings. Barjastehmaleki et al. [18] studied the statistical structure of turbulence pressure fluctuations caused by hydraulic jumps with the stilling basins. Barjastehmaleki et al. [19] evaluated an approach for the structural design of stilling basins lining in the sealed and unsealed joints. Lopardo [20] recommends that certain flow conditions are fulfilled when measuring pressure fluctuations. The supercritical Reynolds number (Re_1) should be more than 100,000. The minimum acquisition time must be 60 seconds. The acquisition frequency can be considered between 50 and 100 Hz. The maximum length of the plastic tube between the pressure tap and transducer is equal to 55 cm with a minimum inner diameter of 5 mm.

There are some pressure estimation methodologies associated with the hydraulic jumps in the literature. Gu et al. [21] evaluated the SPH model to estimate the wave profile, velocity data, and energy dissipation caused by hydraulic jumps. Güven et al. [22] used neural networks to predict the pressure fluctuations on the bed of a sloping stilling basin under B-type hydraulic jump, was investigated in detail by Hager [23]. Teixeira [24] determined the extreme pressures with different non-exceedance probabilities $P^*_{a\%}$ from the sample data within a stilling basin. Teixeira et al. [25] provided the cumulative curves of $P^*_{a\%}$ for characteristic points along the hydraulic jump. Souza et al. [26] investigated the behavior of the hydraulic jump concerning the longitudinal distribution of pressures near the bottom of the basin in the low Froude number zone ($Fr_1 \leq 4.5$). Dai Prá et al. [27] investigated the influence of the vertical curve between the spillway chute and the stilling basin bottom. Maximum pressure fluctuations were identified at the center of the vertical curve and assume values of 1% of the flow kinetic energy at the terminal tangency point of the curve. Novakoski et al. [28] investigated extreme pressures with different non-exceedance probabilities ($P^*_{0.1\%}$, $P^*_{1\%}$, $P^*_{99\%}$, and $P^*_{99.9\%}$). This study was carried out on a dissipation basin downstream of a stepped spillway. The results showed that the values of $P^*_{0.1\%}$ and $P^*_{99.9\%}$ have lower and higher values than the same values observed downstream of the smooth chute, in the region near to the spillway toe, respectively.

According to Marques et al. [29], the pressure distributions along the hydraulic jumps are not described by a normal distribution. The distributions of the skewness (S) and kurtosis (K) coefficients of the sample pressure data along the hydraulic jump differ significantly from the values 0 and 3, respectively, attributed to a normal distribution. Such values are observed after the endpoint of the hydraulic jump at the dimensionless position $X^* \approx 8$. According to Marques et al. [29], the distances are made dimensionless concerning the conjugate depths, i.e., $X^* = X/(Y_2 - Y_1)$. Analysis of skewness and kurtosis displays that there are several types of distributions along hydraulic jumps. Therefore, it is difficult to estimate the pressure data with a certain non-exceedance probability ($P^*_{a\%}$). They proposed dimensionless relationships linking pressures with a certain non-exceedance probability ($P^*_{a\%}$), to the mean pressure (P^*_m), and the standard deviation of the sample data (σ^*_X). Such relationships allow us to organize the results of different flow discharges or Froude numbers and characterize the interest points in hydraulic jumps. The characteristic points are (i) the maximum pressure fluctuations point ($X^*_{\sigma max}$); (ii) the point of the flow detachment (X^*_d); (iii) the endpoint of the roller (X^*_r); (iv) the endpoint of the hydraulic jump (X^*_j). These points are located at positions around 1.75, 4.0, 6.0, and 8.0, respectively.

The focus of this study is the statistical analysis of the extreme pressures distribution at the bottom of a smooth stilling basin for the incident Froude numbers (Fr_1) ranging from 6.14 to 8.29. A

new adjustment will be proposed for the dimensionless standard deviation (σ^*x) based on Teixeira [24] to estimate the extreme pressures with different non-exceedance probabilities ($P^*_{a\%}$).

2. Materials and Methods

2.1. Experimental setup and procedure

Pressure patterns along free hydraulic jumps acting on the bottom of the USBR Type I stilling basin (smooth bed) downstream of an Ogee spillway, were investigated using a laboratory model (Figure 1). The experiments were conducted in a laboratory Plexiglas-walled flume with 50 cm width, 60 cm height, and 10 m length in the hydraulic laboratory at the University of Tabriz, Iran. The flume bed was horizontal. An Ogee spillway with 70 cm height (P), and 61 cm length (L) was equipped with a Type I stilling basin according to the USBR recommendations [30].

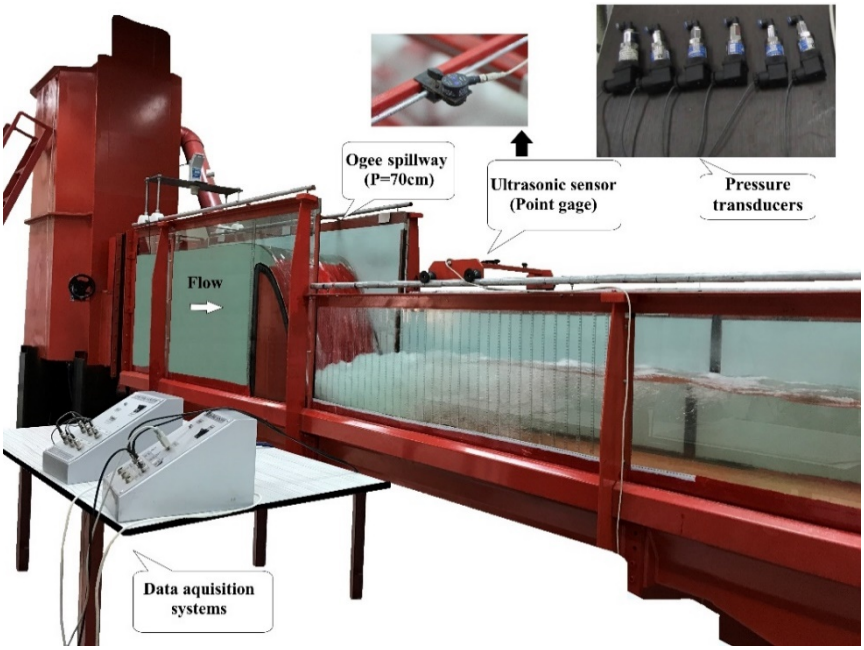

Figure 1. Laboratory flume and the experimental setup.

The length of the USBR Type I stilling basin (L_b) was considered 200 cm [31]. The basin width (B) was equal to the flume width (50 cm). The radius of the vertical curve (R) at the spillway toe was 12 cm. There was a head tank with 250 cm height to stabilize the flow upstream of the spillway. A hinged weir downstream of the flume was used to control the position of the supercritical depth (Y_1) at the spillway toe. The sequent depth (Y_2) was measured by an ultrasonic sensor, with an operating in the range of 10 to 100 cm and an accuracy of ±0.1 mm. The supercritical depth (Y_1) was calculated using Bélanger's equation for the classical hydraulic jump [32-34]:

$$\frac{Y_1}{Y_2} = \frac{1}{2}\left(-1+\sqrt{1+8Fr_2^2}\right) \quad (1)$$

$$V_2 = \frac{q}{Y_2} \quad (2)$$

$$Fr_2 = \frac{V_2}{\sqrt{g.Y_2}} \quad (3)$$

where V_2 is the mean sequent velocity; q is the flow discharge per unit width; Fr_2 is the sequent Froude number; and g is the gravitational acceleration. The flow discharge (Q) was measured with an ultrasonic flowmeter. Experiments were carried out with different flow discharges in the range of 33

Preprints (www.preprints.org) | NOT PEER-REVIEWED | Posted: 26 January 2020 doi:10.20944/preprints202001.0310.v1

Peer-reviewed version available at Mathematics 2020, 8, 323; doi:10.3390/math8030323

to 60.4 L/s. Table 1 presents the range of some experimental parameters along the hydraulic jumps. The parameters in Table 1 are defined as follows [33]:

$$V_1 = \frac{q}{Y_1} \tag{4}$$

$$Fr_1 = \frac{V_1}{\sqrt{g.Y_1}} \tag{5}$$

$$Re_1 = \frac{V_1.R_1}{\nu} \tag{6}$$

Table 1. Experimental parameters along the hydraulic jumps.

Q (L/s)	Y_1 (cm)	Y_2 (cm)	V_1 (m/s)	V_2 (m/s)	Fr_1 (–)	Fr_2 (–)	Re_1 (–)
33.0	1.84	20.65	3.52	0.313	8.29	0.220	58200
43.0	2.35	23.70	3.59	0.356	7.48	0.233	74400
47.5	2.59	24.87	3.60	0.374	7.14	0.240	81500
52.7	2.89	26.05	3.58	0.397	6.72	0.248	89500
55.0	3.03	26.49	3.56	0.407	6.52	0.253	92900
60.4	3.36	27.55	3.53	0.430	6.14	0.261	100900

where V_1 is the mean incident velocity; Fr_1 and Re_1 are the incident Froude and Reynolds numbers, respectively); R_1 is the hydraulic radius of the initial flow; and ν is the kinematic viscosity of the fluid. Figure 2 shows a schematic view of the experimental setup, and the distribution of pressure taps along the centerline of the stilling basin.

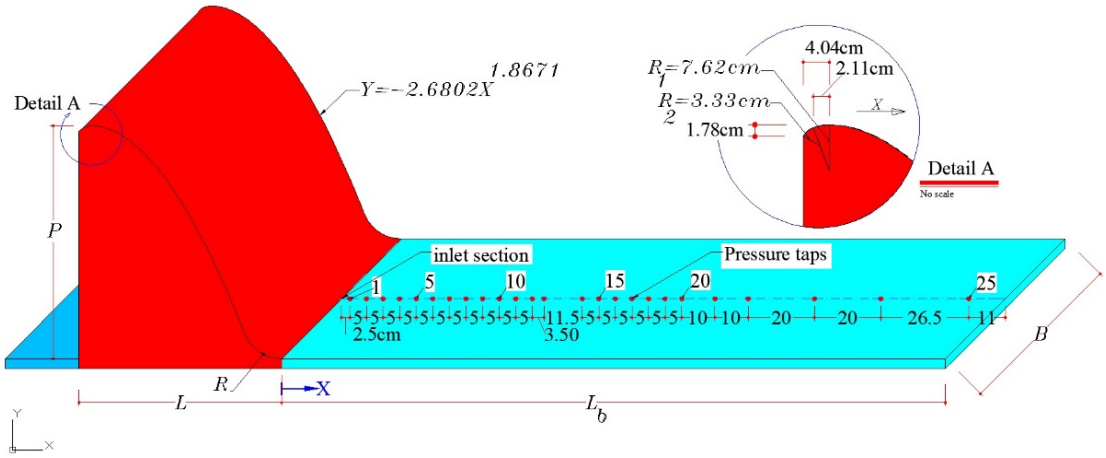

Figure 2. Schematic view of the experimental setup, and the distribution of pressure taps along the stilling basin.

To measure the instantaneous pressure data, 25 pressure taps were installed at the bottom, along the centerline of the stilling basin. Afterward, these data were converted into electrical signals by pressure transducers via a 6-channel digital board. In this study, the transparent plastic tubes were used with an inner diameter of 3 mm, and the maximum lengths of 200 cm. The six Atek transducers (model BCT- 110) had an operating range of –100 to 100 cm of the water column, with an accuracy of ±0.2%. The data acquisition frequency of 20 Hz with a duration of 90 seconds was used to collect 1800 sample data for each test and each pressure tap. After processing the signals using a data acquisition system, the recorded data were displayed using the 6-CH Pressure DAQ software.

Preprints (www.preprints.org) | NOT PEER-REVIEWED | Posted: 26 January 2020 doi:10.20944/preprints202001.0310.v1

Peer-reviewed version available at Mathematics 2020, 8, 323; doi:10.3390/math8030323

2.2. Statistical Data Analysis

A series of methodologies to estimate hydraulic pressures under different conditions were used in the literature. Pressure with a certain non-exceedance probability ($P_{a\%}$) can be estimated using equation (7):

$$P_{a\%} = P_m + N_{a\%}.\sigma_X \tag{7}$$

where $P_{a\%}$ is the pressure value with a certain non-exceedance probability at point X; P_m is the mean pressure at point X (in cm or m of water); $N_{a\%}$ is the dimensionless statistical coefficient of the probability distribution at point X; σ_X is the standard deviation at the point X (in cm or m of water); and X is the longitudinal distance of each pressure tap from the spillway toe. According to Marques et al. [29], the dimensionless mean pressure (P^*_m), and the dimensionless pressure with a certain non-exceedance probability ($P^*_{a\%}$) can be expressed as a generic function of X^*, and defined as follows:

$$P^*_m = \frac{P_m - Y_1}{Y_2 - Y_1} = f(X^*) \tag{8}$$

$$P^*_{a\%} = \frac{P_{a\%} - Y_1}{Y_2 - Y_1} = f'(X^*) \tag{9}$$

Pressure fluctuations within the hydraulic jumps are related to energy dissipation. According to Marques et al. [29], the dimensionless standard deviation (σ^*_X) is defined as follows:

$$\sigma^*_X = \frac{\sigma_X}{\Delta H}.\frac{Y_2}{Y_1} = f''(X^*) \tag{10}$$

$$\Delta H = (Y_1 + \frac{V_1^2}{2g}) - (Y_2 + \frac{V_2^2}{2g}) \tag{11}$$

where ΔH is the energy dissipation along the hydraulic jump (cm or m). This parameter depends on the incident Froude number (Fr_1), and the distance of the point from the jump toe. Based on equation (7), Teixeira [24] proposed an estimation methodology for the extreme pressures with different non-exceedance probabilities ($P^*_{a\%}$) along free hydraulic jumps for smooth stilling basins, downstream of a smooth chute spillway. The method is applied to stable hydraulic jumps ($4.5 < Fr_1 < 9$), and includes the assessment of the dimensionless statistical parameters (mean pressures, standard deviation, and statistical probability distribution coefficient) as a function of X^* along stilling basins with a smooth bed. These relationships are defined as follows:

$$P^*_X = -0.015X^{*2} + 0.237X^* + 0.07 \qquad 0 \le X^* \le 8 \tag{12}$$

$$\sigma^*_X = -0.159X^{*2} + 0.573X^* + 0.19 \qquad 0 \le X^* \le 2.4 \tag{13}$$

$$\sigma^*_X = 0.017X^{*2} - 0.281X^* + 1.229 \qquad 2.4 \le X^* \le 8.25 \tag{14}$$

$$N_{a\%} = a.X^{*2} + b.X^* + c \qquad 0 \le X^* \le 8 \tag{15}$$

The parameters of a, b, and c vary according to the extreme pressures with different non-exceedance probabilities, as resumed in Table 2 [24].

Table 2. Parameters of a, b and c to estimate $N_{a\%}$ [24].

$\alpha\%$	α	b	c	R^2
1%	0.0512	–0.4480	–1.6601	0.92
5%	0.0130	–0.1323	–1.3061	0.73

Preprints (www.preprints.org) | NOT PEER-REVIEWED | Posted: 26 January 2020 doi:10.20944/preprints202001.0310.v1

Peer-reviewed version available at Mathematics 2020, 8, 323; doi:10.3390/math8030323

10%	0.0032	−0.0450	−1.0869	0.59
90%	0.0048	−0.0325	1.2695	0.26
95%	0.0171	−0.1393	1.8624	0.81
99%	0.0317	−0.3598	3.3008	0.86

The spatial patterns of the skewness coefficient (S) may be used to highlight the flow detachment in different zones. The sample skewness coefficient is defined as follows [29]:

$$S = \frac{n}{(n-1).(n-1)} . \frac{\sum_{i=1}^{n} (P_i - P_m)^3}{S_X^3} = f'''(X^*) \quad (16)$$

$$S_X = \sqrt{\frac{\sum_{i=1}^{n} (P_i - P_m)^2}{(n-1)}} \quad (17)$$

where P_i is the instantaneous pressure head at each pressure tap (in cm or m of water); S_X is the sample standard deviation; and n is the number of sample data. The mean pressure (P_m) corresponds to the arithmetic mean of the sample pressure data collected by each transducer for each test and each pressure tap. Similarly, the standard deviation of the sample data (S_X) was calculated. This value represents the pressure fluctuations concerning the mean pressure of the sample data. A value of $S > 0$ indicates the presence of the pressure data higher than the mean pressure value, moving the density probability function (PDF) of the pressure fluctuations towards the right, and vice versa for $S < 0$.

The patterns of the kurtosis coefficient (K) in the hydraulic jump confirm the results of the analysis of the pressure fluctuations (σ^*_X). The value of K is a measure of the spread of data around the mean value, characterizing the flatness of the PDF curve. A value of $K < 3$ indicates the data distribution function is more flattened and less concentrated to the mean values compared to a normal distribution, and vice versa for $K > 3$. The sample kurtosis coefficient is defined as [29]:

$$K = \frac{n.(n+1)}{(n-1).(n-2).(n-3)} . \frac{\sum_{i=1}^{n} (P_i - P_m)^4}{S_X^4} = f''''(X^*) \quad (18)$$

The statistical analysis of sample pressure data consisted of calculating the values of P_m, σ_X, $P_{a\%}$, and $N_{a\%}$. From the analysis of the probability distribution of sample pressure data, the pressure data with different non-exceedance probabilities ($P_{a\%}$) were determined. Then, the dimensionless form of pressure data ($P^*_{a\%}$) was taken to compare the results with different arrangements, obtained from a series of data with different geometries. These parameters were analyzed longitudinally, along the stilling basin, and were made dimensionless using equations (8) to (10), respectively.

Based on Teixeira [24], the corresponding estimates of the dimensionless statistical parameters were determined using equations (12) to (15) and Table (2). Afterward, the dimensional form of the mean pressure (P_m) and standard deviation (σ_X) were calculated using equations (8) and (10), respectively. Finally, the estimated pressure with a certain non-exceedance probability ($P_{a\%}$) was calculated using equation (7). To optimize the pressure estimation methodology proposed by Teixeira [24], a new third-order adjustment was developed for the dimensionless standard deviation (σ^*_X), as a function of X^* along the stilling basin. The results of $P^*_{a\%}$, obtained from the analysis of the probability distribution of the experimental data were compared with the corresponding estimated values using the methodology by Teixeira [24], and the new optimized estimation methodology proposed in this study.

2.3. Statistical performance criteria

To evaluate the performance of the experimental and the estimated standard deviation (σ^*_X), some statistical performance criteria are defined as follows:

I: Determination coefficient (R^2) [35]:

Preprints (www.preprints.org) | NOT PEER-REVIEWED | Posted: 26 January 2020 doi:10.20944/preprints202001.0310.v1

Peer-reviewed version available at Mathematics 2020, 8, 323; doi:10.3390/math8030323

$$R^2 = \left(\frac{n.\sum_{i=1}^{2}(x_i.y_i) - (\sum_{i=1}^{n}x_i).(\sum_{i=1}^{n}y_i)}{\sqrt{n.\sum_{i=1}^{n}x_i^2 - (\sum_{i=1}^{n}x_i)^2}.\sqrt{n.\sum_{i=1}^{n}y_i^2 - (\sum_{i=1}^{n}y_i)^2}}\right)^2 \quad (19)$$

II: Root Mean Squared Error (RMSE) [35]:

$$RMSE = \sqrt{\frac{\sum_{i=1}^{n}(x_i - y_i)^2}{n}} \quad (20)$$

III: Mean Absolute Error (MAE) [36]:

$$MAE = \frac{\sum_{i=1}^{n}|x_i - y_i|}{n} \quad (21)$$

IV: Willmott's Index of Agreement (WI) [37]:

$$WI = 1 - \frac{\sum_{i=1}^{n}(x_i - y_i)^2}{\sum_{i=1}^{n}(|x_i - \bar{x}_i| + |y_i - \bar{x}_i|)^2} \quad (22)$$

where x_i and y_i are the i^{th} experimental, and the estimated standard deviation ($\sigma^* x$), respectively; $\bar{x}_i$ is the mean value of x_i; and n is the total number of data. For proper performance, RMSE and MAE should be close to zero; and R^2 and WI values should be close to the unit.

3. Results and Discussion

3.1. Skewness and Kurtosis Coefficient

According to Figures 3 and 4, from the analysis of the skewness coefficient (S) and kurtosis coefficient (K), as a function of X^* for six Froude numbers, it is found that the pressure distribution along the stilling basin does not follow a normal distribution.

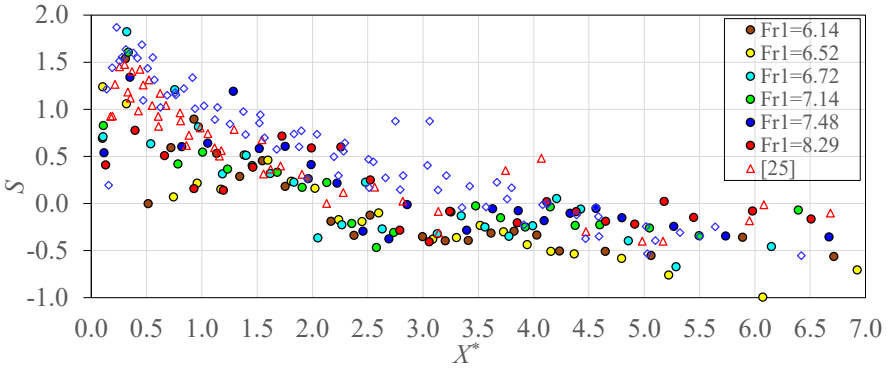

Figure 3. Skewness coefficient along the stilling basin.

Preprints (www.preprints.org) | NOT PEER-REVIEWED | Posted: 26 January 2020 doi:10.20944/preprints202001.0310.v1

Peer-reviewed version available at Mathematics 2020, 8, 323; doi:10.3390/math8030323

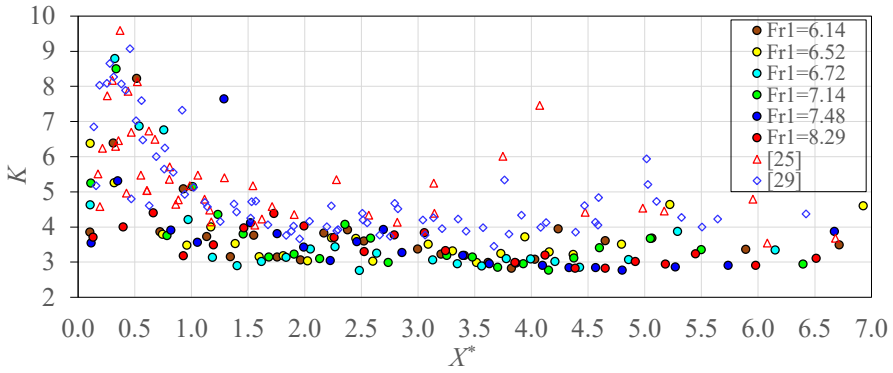

Figure 4. Kurtosis coefficient along the stilling basin.

From S and K charts, some characteristic points of the hydraulic jump could be defined. These are the point with the maximum pressure fluctuations ($X^*_{\sigma max}$), where the skewness coefficient is high, and S_{max} is in the range of 0.5 to 1.5. The position of the flow detachment (X^*_d), where the skewness coefficient shifts from a positive value to a negative one ($S \approx 0$); the endpoint of the roller (X^*_r) indicates the minimum skewness coefficient (S_{min}); and endpoint of the hydraulic jump (X^*_j) is where the streamlines become parallel to the bottom of the stilling basin, and S values increase to reach values close to zero. After this position, $S \approx 0$ and $K \approx 3$. According to Marques et al. [29], the approximate positions of the characteristic points $X^*_{\sigma max}$, X^*_d, X^*_r, and X^*_j along the stilling basin for different Froude numbers are provided in Table 3.

Table 3. Approximate positions of the characteristic points along the stilling basin.

Fr_1	$X^*_{\sigma max}$	X^*_d	X^*_r	X^*_j
8.29	1.993	4.120	5.449	6.512
7.48	1.756	3.864	5.737	6.674
7.14	1.683	3.927	5.498	6.396
6.72	1.619	3.994	6.152	7.016
6.52	1.812	4.156	6.075	6.927
6.14	1.757	4.030	5.890	6.717

3.2. Cumulative Pressure Curves

From the pressure data with different non-exceedance probabilities ($P^*_{a\%}$), the cumulative pressure curves were provided for each pressure tap with different Froude numbers. Figure 5 presents the cumulative pressure curves for $P^*_{a\%}$ related to the characteristic points of $X^*_{\sigma max}$, X^*_d, X^*_r, and X^*_j, respectively. It is evident that pressure values ($P^*_{a\%}$) increase with increasing non-exceedance probability ($a\%$). Minimum pressure data (P^*_{min}) correspond to the lowest non-exceedance probabilities ($P^*_{1\%}$). On the contrary, maximum pressure data (P^*_{max}) correspond to the highest non-exceedance probability ($P^*_{99\%}$). Accordingly, the maximum pressure fluctuations, as well as the negative pressures, are located at the positions closest to the spillway toe. Also, the minimum pressure fluctuations are located at the positions downstream of the hydraulic jump.

Preprints (www.preprints.org) | NOT PEER-REVIEWED | Posted: 26 January 2020 doi:10.20944/preprints202001.0310.v1

Peer-reviewed version available at Mathematics 2020, 8, 323; doi:10.3390/math8030323

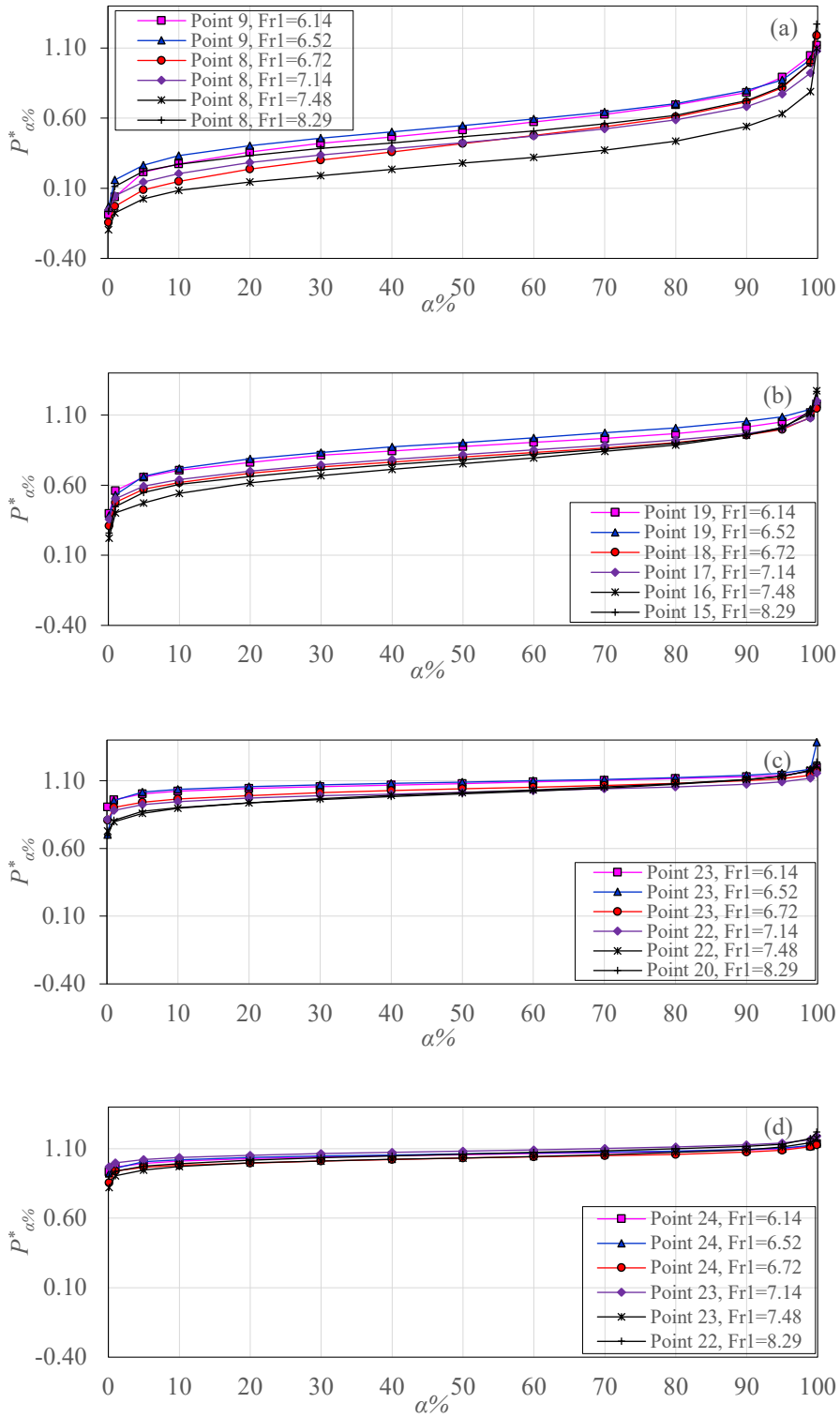

Figure 5. Cumulative pressure curves for $P^*_{\alpha\%}$ related to the characteristic points of the hydraulic jump: (a) $X^*_{\sigma max}$, (b) X^*_d, (c) X^*_r, and (d) X^*_j.

3.3. Proposition of New Adjustment

Based on the results obtained, it was observed that the methodology proposed by Teixeira [24] could be optimized to be used for present data, or in similar conditions by using another relationship

Preprints (www.preprints.org) | NOT PEER-REVIEWED | Posted: 26 January 2020 doi:10.20944/preprints202001.0310.v1

Peer-reviewed version available at Mathematics 2020, 8, 323; doi:10.3390/math8030323

for the dimensionless standard deviation (σ^*x). Thus, a third-order polynomial relationship, as a function of the dimensionless position along the stilling basin, is introduced.

$$\sigma_X^* = 0.011X^{*3} - 0.1565X^{*2} + 0.5379X^* + 0.3036 \qquad 0 \le X^* \le 7 \qquad (23)$$

Figure 6 shows the corresponding scatter plot of σ^*x, and fitting of equation (23), with a determination coefficient (R^2) equal to 0.717.

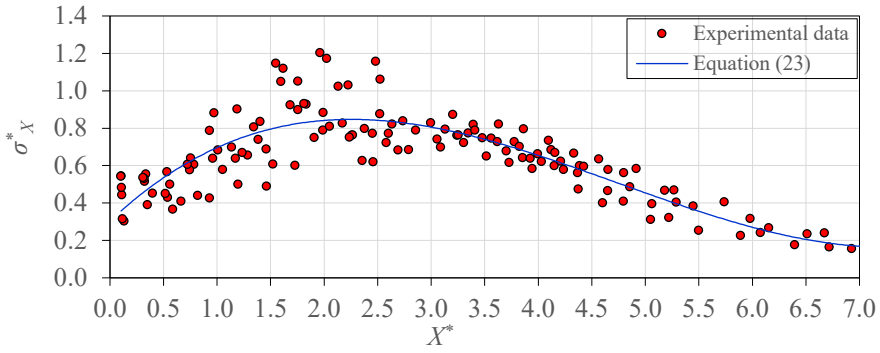

Figure 6. Distribution of σ^*x as a function of X^*, including the experimental data and Equation (23).

3.4. Comparison between Sample and Estimated Pressure Data

Figure 7 presents the distributions of $P^*_{a\%}$ with non-exceedance probabilities of 1%, 5%, 10%, 90%, 95%, and 99%. Experimental data are presented as a function of X^*, together with the corresponding estimates using Teixeira [24], also modified using equation (23).

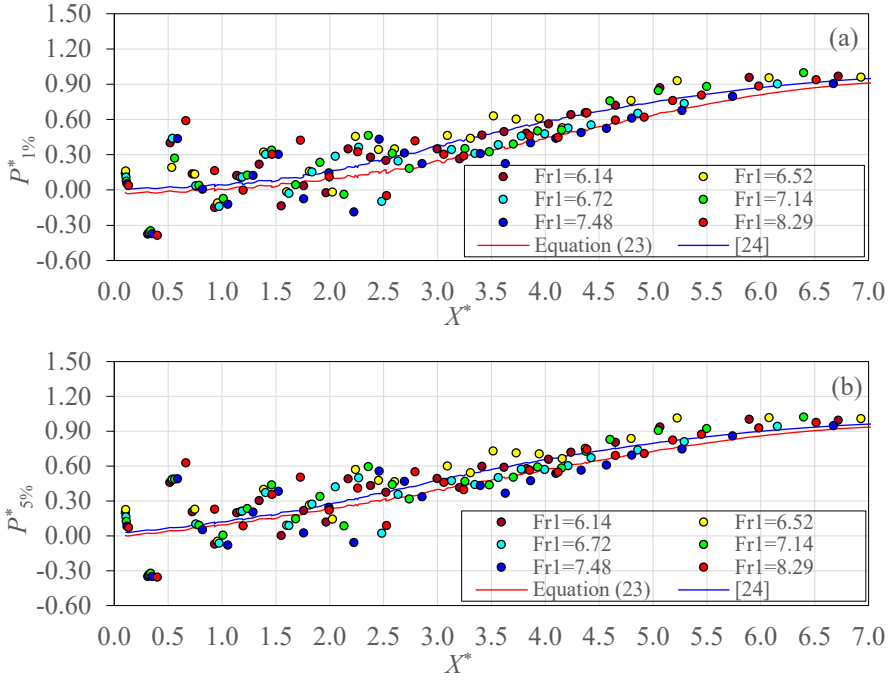

Figure 7. Distributions of $P^*_{a\%}$ with different non-exceedance probabilities: (a) $P^*_{1\%}$, (b) $P^*_{5\%}$, (c) $P^*_{10\%}$, (d) $P^*_{90\%}$, (e) $P^*_{95\%}$, (f) $P^*_{99\%}$.

Preprints (www.preprints.org) | NOT PEER-REVIEWED | Posted: 26 January 2020 doi:10.20944/preprints202001.0310.v1

Peer-reviewed version available at Mathematics 2020, 8, 323; doi:10.3390/math8030323

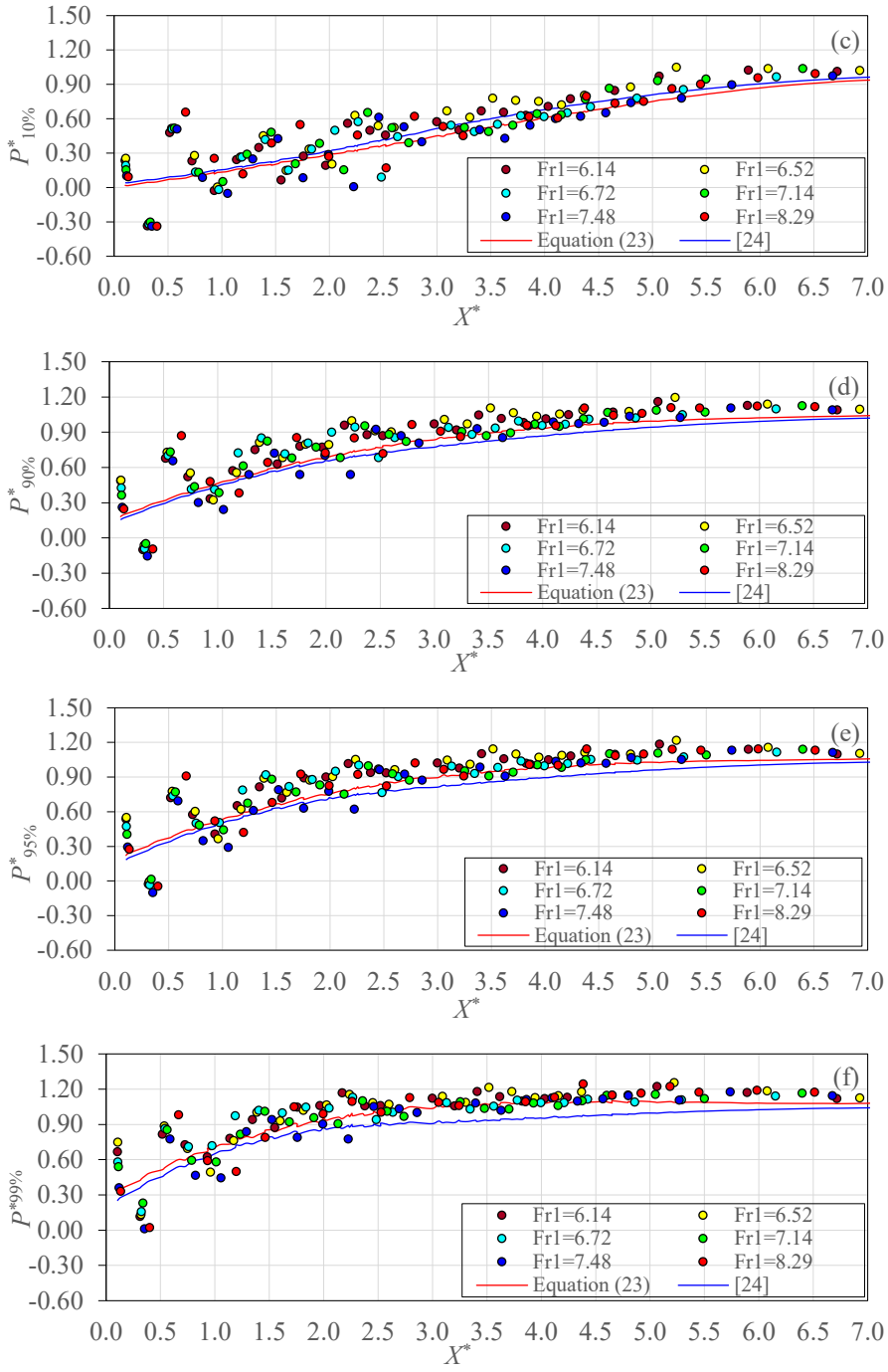

Figure 7. Cont.

Accordingly, close to the spillway toe pressures with low and high non-exceedance probability, especially for $P^*_{1\%}$ and $P^*_{99\%}$, have lower and higher values, with the maximum differences than P^*_m. $P^*_{1\%}$ data reach negative values down to –0.2, at the position $X^* \approx 2$, indicating regions with low pressures. The goodness of fit statistics for the estimation of σ^*_X is provided in Table 4.

Table 4. Results of the statistical performance criteria for σ^*_X.

Methodology	R2	RMSE	MAE	WI
Equation (23)	0.717	0.119	0.088	0.911
[24]	0.609	0.224	0.192	0.738

As one can see in Figure7, both methodologies accommodate experimental data ($P^*_{a\%}$) with acceptable accuracy. However, the estimates of $P^*_{1\%}$, $P^*_{5\%}$, and $P^*_{10\%}$ display some differences between experimental and estimates. The new methodology is given in equation (23) presents somewhat better results for $P^*_{90\%}$, $P^*_{95\%}$, and $P^*_{99\%}$ along the stilling basin. This adjustment for dimensionless standard deviation (σ^*_X) provides better estimation performance as compared against Teixeira [24], as reported in Table 4.

4. Conclusions

In this study, extreme pressures beneath hydraulic jumps inside the USBR Type I stilling basin (smooth bed) downstream of an Ogee spillway, are investigated for different incident Froude numbers ranging from 6.14 to 8.29. In summary, several conclusions are provided as follows:

i. Sample skewness (S) and kurtosis (K) coefficients indicated that the pressure distribution along the hydraulic jumps does not follow a normal distribution. Some characteristic points of the hydraulic jump are the maximum pressure fluctuations point ($X^*_{\sigma max}$) with S_{max}; the flow detachment point (X^*_d) with $S \approx 0$; the roller endpoint (X^*_r) with S_{min}; and the hydraulic jump endpoint (X^*_j) with $S \approx 0$.

ii. From the pressure data with different non-exceedance probabilities ($P^*_{a\%}$), the cumulative pressure curves are presented for $P^*_{a\%}$ related to the characteristic points of $X^*_{\sigma max}$, X^*_d, X^*_r, and X^*_j, respectively. For the positions close to the spillway toe, pressures with low and high non-exceedance probability ($P^*_{1\%}$ and $P^*_{99\%}$), have lower and higher values, with the maximum differences than P^*_m. $P^*_{1\%}$ data reach negative values down to –0.2, at the position $X^* \approx 2$, indicating regions with low pressures.

iii. From the analysis of the probability distribution of the sample data as collected by pressure transducers, pressures with certain non-exceedance probabilities ($P^*_{a\%}$) can be determined.

iv. Based on the results obtained, it was observed that the methodology proposed by Teixeira [24] could be optimized to be used for present data, or in similar conditions by using another relationship for the dimensionless standard deviation (σ^*_X). Thus, a third-order polynomial relationship, as a function of the dimensionless position along the stilling basin (X^*), is introduced. This adjustment is valid for the dimensionless positions (X^*) in the range of 0 to 7.

v. To assess the accuracy of this adjustment, some performance criteria are used, including determination coefficient (R^2), root mean square error (RMSE), mean absolute error (MAE), and Willmott's index of agreement (WI). For the new proposed adjustment in this study, the values of R^2, RMSE, MAE, and WI were achieved 0.717, 0.119, 0.088, and 0.911, respectively. This modified methodology has better results for maximum extreme pressure data, i.e., those with non-exceedance probabilities of 90%, 95%, and 99%. The new adjustment for σ^*_X should be validated against sample data taken in similar conditions to our case study here.

Conflicts of Interest: The authors declare no conflict of interest.

Notation

The following symbols are used in this paper:

a, b, c	Parameters of the second-order polynomial relationship for $N_{a\%}$
B	Basin width (L)
Fr_1	Incident Froude number
Fr_2	Sequent Froude number
g	Gravitational acceleration (LT^{-2})
K	Kurtosis coefficient
L	Spillway length (L)
L_b	Length of the USBR Type I stilling basin (L)
MAE	Mean Absolute Error
n	Total number of data

$N_{a\%}$	Statistical coefficient of probability distribution at point X
P	Spillway height (L)
$P_{a\%}$	Pressure with a certain non-exceedance probability (L)
$P^*_{a\%}$	Dimensionless pressure with a certain non-exceedance probability
P_i	Instantaneous pressure of each pressure tap (L)
P_m	Mean pressure of each pressure tap (L)
P^*_m	Dimensionless mean pressure of each pressure tap
Q	Flow discharge (L^3T^{-1})
q	Flow discharge per unit width (L^2T^{-1})
R_1	Hydraulic radius of the incoming flow (L)
R^2	Determination coefficient
Re_1	Incident Reynolds number
RMSE	Root Mean Squared Error
S	Skewness coefficient
S_X	Sample standard deviation
V_1	Mean incident velocity (LT^{-1})
V_2	Mean sequent velocities (LT^{-1})
WI	Willmott's index of agreement
x_i	i^{th} measured value of $P^*_{a\%}$
$\bar{x}_i$	Average value of x_i
X	Distance of each pressure tap from the spillway toe (L)
X^*	Dimensionless distance of each pressure tap from the spillway toe, i.e., $X/(Y_2 - Y_1)$
X^*_d	Point of the flow detachment, i.e., $X_d/(Y_2 - Y_1)$
X^*_j	Endpoint of the hydraulic jump, i.e., $X_j/(Y_2 - Y_1)$
X^*_r	Endpoint of the roller, i.e., $X_r/(Y_2 - Y_1)$
$X^*_{\sigma max}$	Point of the maximum pressure fluctuations, i.e., $X_{\sigma max}/(Y_2 - Y_1)$
Y_1	Supercritical depth (L)
Y_2	Sequent depth (L)
y_i	i^{th} estimation value of $P^*_{a\%}$
ΔH	Energy dissipation along the hydraulic jump (L)
ν	Kinetic viscosity of the fluid (L^2T^{-1})
σx	Standard deviation of the experimental data (or pressure fluctuations) at point x (L)

Subscripts

1	supercritical flow
2	subcritical sequent flow
m	mean value
max	maximum value
min	minimum value

Contribution:

Conceptualization, Narjes Nabipour, Amir Mosavi and Shahaboddin Shamshirband; Data curation, Renato Steinke Júnior and Eder Daniel Teixeira; Formal analysis, Renato Steinke Júnior and Narjes Nabipour; Funding acquisition, Shahaboddin Shamshirband; Investigation, Eder Daniel Teixeira and Narjes Nabipour; Methodology, Seyed Nasrollah Mousavi and Daniele Bocchiola; Resources, Seyed Nasrollah Mousavi; Software, Eder Daniel Teixeira and Daniele Bocchiola; Supervision, Seyed Nasrollah Mousavi and Shahaboddin Shamshirband; Validation, Daniele Bocchiola; Writing – original draft, Amir Mosavi; Writing – review & editing, Amir Mosavi and Shahaboddin Shamshirband.

Declaration: Authors declare no conflict of interests.

References

1. Bukreev, V. Statistical characteristics of the pressure fluctuation in a hydraulic jump. *Journal of Applied Mechanics and Technical Physics* **1966**, *7*, 97-99.
2. Locher, F.A. *Some Characteristics of Pressure Fluctuations on Low-ogee Crest Spillways Relevant to Flow-induced Structural Vibrations*; IOWA INST OF HYDRAULIC RESEARCH IOWA CITY: 1971.
3. Schiebe, F.R. *The Stochastic Characteristics of Pressure Fluctuations on a Channel Bed Due to the Macroturbulence in a Hydraulic Jump*; University of Minnesota.: 1971.
4. Abdul Khader, M.; Elango, K. Turbulent pressure field beneath a hydraulic jump. *Journal of hydraulic research* **1974**, *12*, 469-489.
5. Lopardo, R.; VERNET, G.; RONALDO, R. Correlación de presiones instantáneas inducidas por un resalto hidraúlico libre y estable. In Proceedings of XI Congreso Latinoamericano de Hidráulica IAHR; pp. 23-34.
6. Toso, J.W.; Bowers, C.E. Extreme pressures in hydraulic-jump stilling basins. *Journal of Hydraulic Engineering* **1988**, *114*, 829-843.
7. Farhoudi, J.; Narayanan, R. Force on slab beneath hydraulic jump. *Journal of Hydraulic Engineering* **1991**, *117*, 64-82.
8. Fiorotto, V.; Rinaldo, A. Turbulent pressure fluctuations under hydraulic jumps. *Journal of Hydraulic Research* **1992a**, *30*, 499-520.
9. Fiorotto, V.; Rinaldo, A. Fluctuating uplift and lining design in spillway stilling basins. *Journal of hydraulic engineering* **1992b**, *118*, 578-596.
10. Armenio, V.; Toscano, P.; Fiorotto, V. On the effects of a negative step in pressure fluctuations at the bottom of a hydraulic jump. *Journal of Hydraulic Research* **2000**, *38*, 359-368.
11. Yan, Z.-m.; Zhou, C.-t.; Lu, S.-q. Pressure fluctuations beneath spatial hydraulic jumps. *Journal of Hydrodynamics* **2006**, *18*, 723-726.
12. Onitsuka, K.; Akiyama, J.; Shige-Eda, M.; Ozeki, H.; Gotoh, S.; Shiraishi, T. Relationship between pressure fluctuations on the bed wall and free surface fluctuations in weak hydraulic jump. In *New Trends in Fluid Mechanics Research*, Springer: 2007; pp. 300-303.
13. Lian, J.; Wang, J.; Gu, J. Similarity law of fluctuating pressure spectrum beneath hydraulic jump. *Chinese Science Bulletin* **2008**, *53*, 2230-2238.
14. Lopardo, R.A.; Romagnoli, M. Pressure and velocity fluctuations in stilling basins. In *Advances in water resources and hydraulic engineering*, Springer: 2009; pp. 2093-2098.
15. Lopardo, R.A. Extreme velocity fluctuations below free hydraulic jumps. *Journal of Engineering* **2013**, *2013*.
16. Wang, H.; Murzyn, F.; Chanson, H. Total pressure fluctuations and two-phase flow turbulence in hydraulic jumps. *Experiments in fluids* **2014**, *55*, 1847.
17. Fiorotto, V.; Barjastehmaleki, S.; Caroni, E. Stability analysis of plunge pool linings. *Journal of Hydraulic Engineering* **2016**, *142*, 04016044.
18. Barjastehmaleki, S.; Fiorotto, V.; Caroni, E. Spillway stilling basins lining design via Taylor hypothesis. *Journal of Hydraulic Engineering* **2016a**, *142*, 04016010.
19. Barjastehmaleki, S.; Fiorotto, V.; Caroni, E. Design of stilling basin linings with sealed and unsealed joints. *Journal of Hydraulic Engineering* **2016b**, *142*, 04016064.

20. Lopardo, R.A. Metodología de estimación de presiones instantáneas en cuencos amortigüadores. In Proceedings of Anales de la Universidad de Chile; pp. ág. 437-455.
21. Gu, S.; Bo, F.; Luo, M.; Kazemi, E.; Zhang, Y.; Wei, J. SPH Simulation of Hydraulic Jump on Corrugated Riverbeds. *Applied Sciences* **2019**, *9*, 436.
22. Güven, A.; Günal, M.; Cevik, A. Prediction of pressure fluctuations on sloping stilling basins. *Canadian Journal of Civil Engineering* **2006**, *33*, 1379-1388.
23. Hager, W.H. B-jump in sloping channel. *Journal of Hydraulic Research* **1988**, *26*, 539-558.
24. Teixeira, E.D. Previsão dos valores de pressão junto ao fundo em bacias de dissipação por ressalto hidráulico. 2003.
25. Teixeira, E.D.; TRIERWEILER NETO, E.; Endres, L.A.M.; Marques, M.G. Análise das flutuações de pressão junto ao fundo em bacias de dissipação por ressalto hidráulico. In Proceedings of SEMINÁRIO NACIONAL DE GRANDES BARRAGENS; pp. 188-198.
26. SOUZA, P.E.d.A.M., Marcelo Giulian; Neto, E.F.T.; TEIXEIRA, E.D. FLUTUAÇÃO DE PRESSÃO EM UM RESSALTO HIDRÁULICO DE BAIXA QUEDA E BAIXO NÚMERO DE FROUDE A JUSANTE DE UM VERTEDOURO. In Proceedings of SEMINÁRIO NACIONAL DE GRANDES BARRAGENS.
27. Prá, M.D.; Teixeira, E.D.; Marques, M.G.; Priebe, P.d.S. Avaliação das Flutuações de Pressão em Ressalto Hidráulico pela Dissociação de Esforços. *Rbrh: Revista Brasileira de Recursos Hídricos. Porto Alegre, RS. Vol. 21, n. 1 (2016), p. 221-331* **2016**.
28. Novakoski, C.K.; Hampe, R.F.; Conterato, E.; Marques, M.G.; Teixeira, E.D. Longitudinal distribution of extreme pressures in a hydraulic jump downstream of a stepped spillway. *RBRH* **2017**, *22*.
29. Marques, M.G.; Drapeau, J.; Verrette, J.-L. Flutuação de pressão em um ressalto hidráulico. *Rbrh: Revista Brasileira de Recursos Hídricos. Porto Alegre*, **1997**, *2*, 45-52.
30. Reclamation, U.S.B.o. *Design of small dams*; US Department of the Interior, Bureau of Reclamation: 1987.
31. Chanson, H.; Carvalho, R. Hydraulic jumps and stilling basins. *Energy Dissipation in Hydraulic Structures; Chanson, H., Ed.; CRC Press: Leiden, The Netherlands* **2015**, 65-104.
32. Rajaratnam, N. Hydraulic jumps. In *Advances in hydroscience*, Elsevier: 1967; Vol. 4, pp. 197-280.
33. Chaudhry, M.H. *Open-channel flow*; Springer Science & Business Media: 2007.
34. Chanson, H. Development of the Bélanger equation and backwater equation by Jean-Baptiste Bélanger (1828). *Journal of Hydraulic Engineering* **2009**, *135*, 159-163.
35. Willmott, C.J.; Matsuura, K. Advantages of the mean absolute error (MAE) over the root mean square error (RMSE) in assessing average model performance. *Climate research* **2005**, *30*, 79-82.
36. Chai, T.; Draxler, R.R. Root mean square error (RMSE) or mean absolute error (MAE)?–Arguments against avoiding RMSE in the literature. *Geoscientific model development* **2014**, *7*, 1247-1250.
37. Willmott, C.J.; Robeson, S.M.; Matsuura, K. A refined index of model performance. *International Journal of Climatology* **2012**, *32*, 2088-2094.